Room-temperature spin coherence in ZnO

S. Ghosh, V. Sih, W. H. Lau, and D. D. Awschalom[a)]
Center for Spintronics and Quantum Computation, University of California, Santa Barbara, California 93106

S.-Y. Bae and S. Wang
Department of Materials Science and Engineering, Stanford University, Stanford, California 94305

S. Vaidya and G. Chapline
Lawrence Livermore National Laboratory, Livermore, California 94550

(Received 23 February 2005; accepted 2 May 2005; published online 3 June 2005)

Time-resolved optical techniques are used to explore electron spin dynamics in bulk and epilayer samples of *n*-type ZnO as a function of temperature and magnetic field. The bulk sample yields a spin coherence time T_2^* of 20 ns at $T=30$ K. Epilayer samples, grown by pulsed laser deposition, show a maximum T_2^* of 2 ns at $T=10$ K, with spin precession persisting up to $T=280$ K. © *2005 American Institute of Physics*. [DOI: 10.1063/1.1946204]

A lot of attention has been focused on zinc oxide (ZnO) because of material properties that make it well suited for applications in ultraviolet light emitters, transparent high-power electronics and piezoelectric transducers. In addition, the theoretical work of Dietl *et al.*,[1] predicting room-temperature ferromagnetism for Mn-doped *p*-type ZnO, has revealed the possibility that ZnO may be an appropriate candidate for spintronics.[2] While the magnetic properties of thin films of ZnO are being widely investigated,[3–5] practical spintronics applications would also require long spin coherence time and spin coherence length.

In this letter, we investigate the electron spin dynamics of nonmagnetically doped *n*-type ZnO. The growth of *p*-type films is an experimental challenge, possibly due to self-compensation from oxygen vacancies[6] or the incorporation of hydrogen as an unintentional donor.[7] Consequently, recent developments reporting magnetic properties in ZnO have been regarding *n*-type samples,[8] although the preparation of *p*-type films has been reported.[9,10] Our measurements on *n*-type ZnO establish a spin coherence time of ~190 ps at room temperature, longer than the spin coherence time reported in GaN,[11] another wide-band-gap semiconductor. ZnO also has the added advantage that high-quality single crystals are commercially available.

We concentrate on four samples—three 100 nm epitaxial thin films (designated as Samples A–C) and a bulk Sample D. The thin films are fabricated by a pulsed laser deposition system using a ceramic ZnO pellet (Praxair Targets, Inc.) as the target and *c*-cut sapphire as the substrate, which is heated to 800 °C during deposition. The substrate *ab* plane is rotated by 30° with respect to that of the epilayers to reduce the lattice mismatch from 16% to 3.85%. Four-circle x-ray diffractometry confirms the single phase growth and the wurtzite structure of ZnO. The oxygen pressure used during the growth process for the epilayers is 10^{-5} Torr (Sample A), 10^{-4} Torr (B), and 10^{-3} Torr (C), which tunes the carrier concentration. Sample D (commercial single crystal from Tokyo-Denpa Company Ltd., grown by hydrothermal method),[12] is mounted on fused silica and polished down to a few microns for transmission measurements.

Transport measurements performed at room temperature show *n*-type conductivity in all four samples. The carrier concentrations (mobilities) for A–D are 1.92×10^{19} cm^{-3} (19 cm^2/Vs), 1.01×10^{19} cm^{-3} (27 cm^2/Vs), 2.64×10^{18} cm^{-3} (37 cm^2/Vs), and 1.26×10^{15} cm^{-3} (240 cm^2/Vs), respectively. We note that Sample D has a carrier concentration several orders of magnitude smaller than the epilayers and a higher mobility.

Time-resolved Faraday rotation (TRFR), an optical pump-probe spectroscopic technique,[13,14] is used to probe the electron spin dynamics. A circularly polarized pump pulse, incident normal to the sample surface, injects spin polarized electrons, and the Faraday rotation angle of a linearly polarized probe pulse, applied after a time delay Δt, measures the projection of the electron spin magnetization as it precesses in a plane perpendicular to the applied transverse magnetic field (Voigt geometry). The pump and probe are typically tuned to 369 nm to address the band gap of ZnO, using the frequency-doubled output from a mode-locked Ti:Sapphire laser with pulse duration ~150 fs and repetition rate of 76 MHz ($t_{rep}=13$ ns). The laser beams are focused to a spot size of ~50 μm, and typical pump and probe powers are 1.9 mW and 200 μW, respectively. The circular polarization of the pump beam is modulated with a photoelastic modulator at 50 kHz for lock-in detection.

TRFR results for Samples A–C at $T=5.5$ K and $B=0.5$ T are shown in Fig. 1. The oscillatory component of the Faraday rotation (θ_F) as a function of time delay is

$$\theta_F(\Delta t) = A\exp(-\Delta t/T_2^*)\cos(\omega_L \Delta t), \quad (1)$$

where A is the amplitude of the electron spin polarization injected perpendicular to B, T_2^* the transverse coherence time and ω_L the Larmor frequency which is related to the electron g-factor g^* by $\hbar\omega_L = g^*\mu_B B$ (where μ_B is the Bohr magneton). Fits to the data in Fig. 1(a) indicate that T_2^* increases with increasing carrier concentration in the epilayers, from 0.5 ns (Sample C) to 2.1 ns (Sample A).

Figures 1(b) and 1(c) show the B dependence of ω_L and T_2^*, respectively. In Fig. 1(b), ω_L increases linearly with B in all samples (including Sample D, not shown here) and we extract a field-independent value of $g^*=1.9$ for the three epilayers, consistent with earlier electron spin resonance

a)Electronic mail: awsch@physics.ucsb.edu

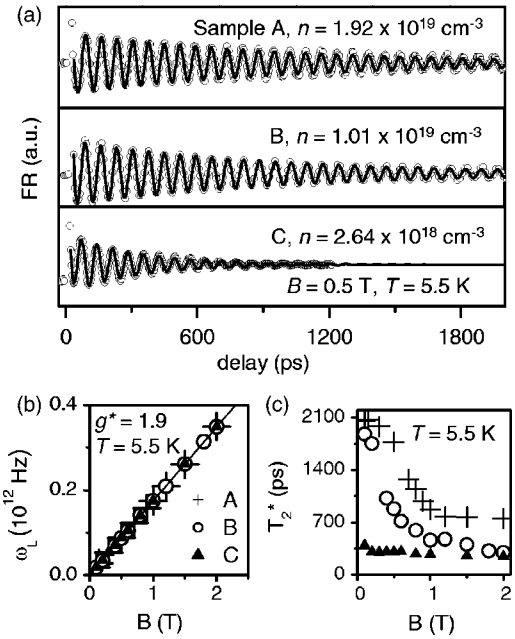

FIG. 1. (a) TRFR as a function of pump-probe delay for the Samples A–C at $T=5.5$ K and $B=0.5$ T. The carrier densities are indicated in the figure. Lines are fits using Eq. (1). (b) Larmor frequency ω_L as a function of B. Line is a linear fit. (c) Spin coherence time T_2^* as a function of B at $T=5.5$ K for the same samples. The symbols in (c) correspond to those in (b).

measurements.[15] This value of g^* is lower than that measured in the bulk Sample D ($g^*=2.03$), which may be attributed to the in-plane compressive strain in the epilayers due to the lattice mismatch with the substrate. Figure 1(c) shows T_2^* decreasing by almost 60% when the magnetic field is increased from $B=0.1$ T to 1 T for Samples A and B, and by about 30% for Sample C. This field dependence is similar to that observed in GaN.[11]

In Fig. 2, we perform a detailed study of the temperature dependence of T_2^* in Sample A, which has the highest carrier density, and the longest spin coherence time of all the epilayers. Figure 2(a) shows the TRFR response at $B=0.8$ T for temperatures $T=80$ K, 180 K and 280 K. The g-factor g^* is temperature independent, while T_2^* decreases with increasing T. Remarkably, spin coherence persists until room temperature, with a spin lifetime of 188 ps at 280 K, considerably longer than the spin coherence time observed in GaN ($\sim$35 ps).[11] Data at $T=280$ K is fit to Eq. (1) plus a nonoscillatory exponential term to account for the fast decay in the initial 25 ps. Figure 2(b) is a logarithmic plot of T_2^* obtained from TRFR data at $B=0.8$ T, as a function of T. For 5.5 K $<T<30$ K, T_2^* is weakly temperature dependent, remaining almost constant at 2 ns; for 30 K $<T<150$ K, it follows a power law $T^{-\alpha}$, with $\alpha=1.54\pm0.03$, for 150 K $<T<290$ K, it is relatively flat, fluctuating around 190 ps.

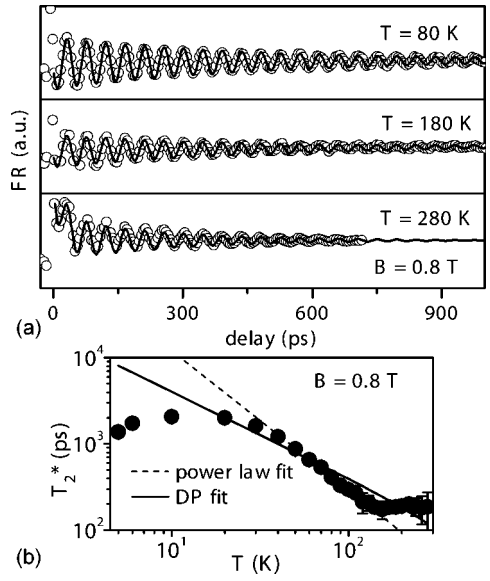

FIG. 2. Temperature dependence of TRFR on Sample A. (a) Spin precession at three temperatures for $B=0.8$ T. (b) T_2^* follows a power law (dashed line) with temperature in the intermediate region of 30 to 150 K, with an exponent -1.54 ± 0.03. Theoretical fit to the data for DP mechanism is shown as a solid line.

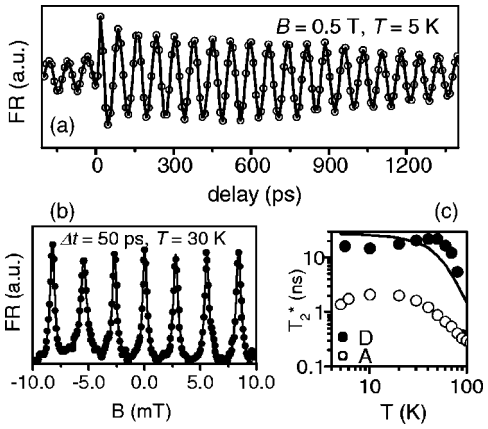

FIG. 3. (a) TRFR at $T=5$ K for the bulk Sample D. Line is a guide for the eyes. (b) Faraday rotation versus B at $T=30$ K and $\Delta t=50$ ps on Sample D showing multiple RSA peaks. Lines are Lorentzian fits. (c) T_2^* obtained from RSA peak at $B=0$ T, as a function of temperature for Sample D (filled circles) with results from Sample A (open circles) shown for comparison. The line is a theoretical fit of the DP mechanism for Sample D.

TRFR data at $T=5$ K and $B=0.5$ T for the bulk Sample D are shown in Fig. 3(a). We observe that the Faraday signal exhibits oscillations at negative delay, indicative of spin magnetization persisting from the previous laser pulse, suggesting $T_2^* \geqslant t_{\mathrm{rep}}$. We employ the method of resonant spin amplification (RSA) which makes it possible to measure spin coherence times well in excess of t_{rep}.[16] Here, the Faraday rotation is measured at a fixed pump-probe delay. By varying the magnetic field, and thus, the Larmor frequency, resonant enhancements in Faraday rotation occur when the spin precession and pulse repetition periods are commensurate, due to constructive interference of successively excited spin packets.

Figure 3(b) shows multiple RSA peaks in a magnetic field scan from +10 mT to −10 mT at $\Delta t=50$ ps and $T=30$ K. From a Lorentzian fit to the zero-field resonance peak, we obtain a T_2^* of 20 ns. Figure 3(c) shows a log-log plot of the temperature dependence of T_2^* in the bulk sample obtained from such fits for 5 K $<T<100$ K. For comparison, we reproduce the temperature dependence of Sample A from Fig. 2(b), and notice that despite having carrier concentration four orders in magnitude lower, T_2^* is larger by a factor of 10 in the bulk. It also does not follow the power law of $T^{-3/2}$ seen in the epilayer. We speculate that these differences between the bulk and the epilayer may be attributed to the presence of compressive strain and higher density of defects in the latter.

Of the three spin decoherence mechanisms relevant in semiconductors—Elliot-Yafet (EY),[17] D'yakonov-Perel (DP),[18] and Bir-Aronov-Pikus (BAP)[19]—the EY process should not be very efficient in ZnO due to its large band gap and small spin-orbit splitting,[20] while the BAP process should only make a significant contribution to the spin relaxation rate when the concentration of holes is high ($\sim 10^{17}$ cm^{-3}). Figures 2(b) and 3(c) (solid lines) show the electron spin relaxation rate for DP process, calculated using $[T_2]^{-1} = 24 m^*_e \gamma_1^2 k_B T \tau_{tr} l\hbar^4 + 256 (m^*_e)^3 \gamma_3^2 E_g (k_B T)^3 \tau_{tr} / 21\hbar^6$, where[21] m^*_e is the electron effective mass, E_g is the band gap, γ_1 and γ_3 are the spin-splitting coefficients, k_B is the Boltzmann constant, and τ_{tr} is the transport time, related to the mobility μ via $\tau_{tr} = \mu m^*_e / q$ (q is the electron charge). While it predicts the correct qualitative trends, it does not explain all of the data, especially the $T^{-3/2}$ dependence and the persisting spin coherence at high temperatures, suggesting that there may be other spin scattering processes responsible for our findings.

In conclusion, we have studied spin coherence in bulk and epilayer samples of ZnO. In the bulk sample, T_2^* extends to very long times at low temperatures. In the epilayers, T_2^* increases with carrier concentration, but is much smaller than in the bulk. However, spin precession in the epilayers persists until room temperature, adding to the attractiveness of ZnO as a material for spintronics.

The authors thank R. J. Epstein and Y. Kato for discussions, and AFOSR, ARO, ONR, and DARPA/DMEA for financial support.

[1] T. Deitl, H. Ohno, F. Matsukura, J. Cibert, and D. Ferrand, Science **287**, 1019 (2000).
[2] S. A. Wolf, D. D. Awschalom, R. A. Buhrman, J. M. Daughton, M. L. Von Molnar, S. Roukes, A. Y. Chtchelkanova, and D. M. Treger, Science **294**, 1488 (2001).
[3] S. J. Pearton, D. P. Norton, K. Ip, Y. W. Heo, and T. Steiner, J. Vac. Sci. Technol. B **22**, 932 (2004).
[4] S. W. Jung, S. J. An, G. C. Yi, C. U. Jung, S. I. Lee, and S. Cho, Appl. Phys. Lett. **80**, 4561 (2002).
[5] T. Fukumura, Z. Jin, M. Kawasaki, T. Shono, T. Hasegawa, S. Koshihara, and H. Koinuma, Appl. Phys. Lett. **78**, 958 (2001).
[6] D. C. Look, J. W. Hemsky, and J. R. Sizelove, Phys. Rev. Lett. **82**, 2552 (1999).
[7] C. G. Van de Walle, Phys. Rev. Lett. **85**, 1012 (2000).
[8] K. Ueda, H. Tabata, and T. Kawai, Appl. Phys. Lett. **79**, 988 (2001).
[9] K. Minegishi, Y. Koiwai, Y. Kikuchi, K. Yano, M. Kasuga, and A. Shimizu, Jpn. J. Appl. Phys., Part 2 **36**, L1453 (1997).
[10] V. Vaithianathan, B. T. Lee, and S. S. Kim, Appl. Phys. Lett. **86**, 062101 (2005).
[11] B. Beschoten, E. Johnston-Halperin, D. K. Young, M. Poggio, J. E. Grimaldi, S. Keller, S. P. DenBaars, U. K. Mishra, E. L. Hu, and D. D. Awschalom, Phys. Rev. B **63**, 121202(R) (2001).
[12] N. Sakagami and K. Shibayama, Jpn. J. Appl. Phys. **20**, 201 (1981).
[13] S. A. Crooker, D. D. Awschalom, J. J. Baumberg, F. Flack, and N. Samarth, Phys. Rev. B **56**, 7574 (1997).
[14] S. A. Crooker, D. D. Awschalom, and N. Samarth, IEEE J. Sel. Top. Quantum Electron. **1**, 1082 (1995).
[15] P. Kasai, Phys. Rev. **130**, 989 (1963).
[16] J. M. Kikkawa and D. D. Awschalom, Phys. Rev. Lett. **80**, 4313 (1998).
[17] R. J. Elliot, Phys. Rev. **96**, 266 (1954).
[18] M. I. D'yakanov and V. I. Perel', Zh. Eksp. Teor. Fiz. **60**, 1954 (1971) [Sov. Phys. JETP **33**, 1053 (1971)].
[19] G. L. Bir, A. G. Aronov, and G. E. Pikus, Zh. Eksp. Teor. Fiz. **69**, 1382 (1975) [Sov. Phys. JETP **42**, 705 (1976)].
[20] O. Madelung, *Semiconductors: Data Handbook* (Springer, Berlin, 2003).
[21] The parameters used in the calculations for $[T_2]_{DP}$ in the epilayers are $\gamma_1 = 0.005$ eV Å, $\gamma_3 = 5$ eV Å^3, $m^*_e = 0.275\, m_e$, and $E_g = 3.445$ eV. In the epilayer, the measured mobility is temperature independent and, for the calculation, we use $\mu(20\text{ K} - 280\text{ K}) = 19$ cm^2/V s, to evaluate τ_{tr}. In the bulk, we use the measured values for the temperature-dependent mobility μ, and tune γ_1 to 0.5 meV Å, to account for the lower strain in the bulk compared to the epilayers.